Science of the Total Environment 739 (2020) 139845

Contents lists available at ScienceDirect

Science of the Total Environment

journal homepage: www.elsevier.com/locate/scitotenv

Carbon dioxide capture in biochar produced from pine sawdust and paper mill sludge: Effect of porous structure and surface chemistry

Avanthi Deshani Igalavithana [a,1], Seung Wan Choi [b,1], Jin Shang [c], Aamir Hanif [c], Pavani Dulanja Dissanayake [a], Daniel C.W. Tsang [d], Jung-Hwan Kwon [e], Ki Bong Lee [b,**], Yong Sik Ok [a,*]

[a] Korea Biochar Research Center, APRU Sustainable Waste Management Program & Division of Environmental Science and Ecological Engineering, Korea University, Seoul 02841, Republic of Korea
[b] Department of Chemical and Biological Engineering, Korea University, Seoul 02841, Republic of Korea
[c] School of Energy and Environment, City University of Hong Kong, Kowloon, Hong Kong, China
[d] Department of Civil and Environmental Engineering, Hong Kong Polytechnic University, Hung Hom, Kowloon, Hong Kong, China
[e] Division of Environmental Science and Ecological Engineering, Korea University, Seoul 02841, Republic of Korea

HIGHLIGHTS

- Pine sawdust biochars showed higher CO_2 adsorption than paper mill sludge biochars.
- Surface area and micro porosity play a vital role in CO_2 adsorption.
- Aromaticity and basic functional groups also facilitate CO_2 adsorption.
- Steam activation enhances CO_2 over N_2 selectivity compared to pristine biochar.

GRAPHICAL ABSTRACT

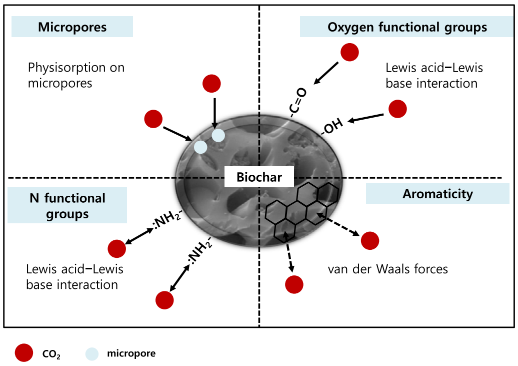

ARTICLE INFO

Article history:
Received 2 March 2020
Received in revised form 24 May 2020
Accepted 29 May 2020
Available online 31 May 2020

Editor: Deyi Hou

Keywords:
CO_2 sequestration
Charcoal
Engineered biochar
Greenhouse gas
Sustainable waste management

ABSTRACT

The CO_2 concentration in the atmosphere is increasing and threatening the earth's climate. Selective CO_2 capture at large point sources will help to reduce the CO_2 emissions to the atmosphere. Biochar with microporous structure could be a potential material to capture CO_2. The impact of feedstock type, pyrolysis temperature and steam activation of biochars were evaluated for CO_2 adsorption capacity. Pine sawdust biochars were produced at 550 °C, and steam activated for 45 min at the same temperature after completing the pyrolysis (PS550 and PSS550). Paper mill sludge biochars were produced at 300 and 600 °C (PMS300 and PMS600). The CO_2 adsorption capacity of biochars was tested at 25 °C using a volumetric sorption analyzer. Pine sawdust biochars showed significantly higher CO_2 adsorption capacity than paper mill sludge biochars due to high surface area and microporosity. Pine sawdust biochars were then evaluated for dynamic adsorption under representative post-combustion flue gas concentration conditions (15% CO_2, 85% N_2) using a breakthrough rig. Both materials showed selective CO_2 uptake over N_2 which is the major component along with CO_2 in flue gas. PSS550 had slightly higher CO_2 adsorption capacity (0.73 mmol $g^{\wedge-1}$ vs 0.67 mmol $g^{\wedge-1}$) and CO_2 over N_2 selectivity (26 vs 18) than PS550 possibly due to increase of microporosity, surface area, and oxygen containing basic functional groups through steam activation. Pine sawdust biochar is an environmentally friendly and low-cost material to capture CO_2.

---

* Corresponding author.
** Corresponding author.
E-mail addresses: kibonglee@korea.ac.kr (K.B. Lee), yongsikok@korea.ac.kr (Y.S. Ok).
[1] These authors contributed equally as first authors.

https://doi.org/10.1016/j.scitotenv.2020.139845

1. Introduction

Global warming is one of the most pressing challenges facing human society due to associated hazardous consequences, such as sea level rising and adverse climatic conditions (Peter, 2018). Mitigation of global warming is a highly debated hot topic in both developing and developed countries (Woolf et al., 2010). Increased concentration of greenhouse gases, mainly CO_2, in the earth atmosphere after the industrial revolution has been identified as the main reason for global warming (Pelletier et al., 2019; Shang et al., 2019). The environmentally non-acceptable level of anthropogenic activities led to breakdown of natural equilibrium of CO_2 among different sinks and sources in atmosphere, lithosphere and hydrosphere (Hanif et al., 2019; Varotsos and Efstathiou, 2019). Hence, efficient and rapid recovery actions such as low emissions and CO_2 capture are essential to reverse the exponentially increasing emission of CO_2 to a reasonable level (Letcher, 2019). Moving towards CO_2 free energy sources such as sunlight, tidal power, wind power and energy carrier of hydrogen is now examined widely to reduce the CO_2 emission via fossil fuel burning, but still the fossil fuel is at the number one as an energy source for many anthropogenic activities (Hansen et al., 2019; Pao and Chen, 2019; Rathore et al., 2019; Staffell et al., 2019). Out of the different anthropogenic sources of CO_2 emission, fossil fuel power plants are the largest one contributing to about 44% of total CO_2 emissions (Yu et al., 2008). Post-combustion technology can be adopted in most power plants, in which CO_2 is selectively captured and removed from the flue gas consisting around 15% CO_2 along with N_2 as the major component (ca. 80%) and other minor components including O_2, NO_x and SO_x (Hanif et al., 2016). Selective CO_2 capture from these large point sources could provide significant benefits to reduce the CO_2 emissions and contents in the atmosphere (Kloutse et al., 2018).

The capturing of CO_2 has been evaluated with various materials such as metal organic frameworks (McDonald et al., 2015), zeolites (Su et al., 2010), carbon based porous materials (Choi et al., 2019; Wang et al., 2013) and silica (Franchi et al., 2005), and these materials showed considerable affinity to adsorb CO_2 even at low concentrations (Jeon et al., 2018). Recently, biochar is evaluated for CO_2 capturing as a carbon material due to its porous structure, surface and structural properties, and easy production methods (Dissanayake et al., 2020a, 2020b; Igalavithana et al., 2019). Also, biochar can be produced from a number of waste materials, such as agricultural wastes, food wastes, and manure at comparatively low temperatures (Igalavithana et al., 2018; Mandal et al., 2017). Biochar exhibited considerably high CO_2 adsorption comparable to the activated carbon at different temperatures and pressures (Kua et al., 2019; Li et al., 2016; Zhang et al., 2015).

In many biochar-utilized CO_2 adsorption studies chemical methods such as KOH activation and ammonia modification have been evaluated to increase the adsorption efficiency (Shafeeyan et al., 2011; Singh et al., 2017; Zhang et al., 2015). Biochar properties can be easily modified by physical modification methods such as alteration of pyrolysis temperature and steam activation; however, very limited studies have been conducted to evaluate the CO_2 adsorption performance using modified biochars (Gargiulo et al., 2018). Therefore, the current study was conducted to evaluate the impact of pyrolysis temperature and steam activation of biochars on CO_2 adsorption. The specific objectives of the study were to 1) evaluate the effect of feedstock on textural, surface, and structural properties of biochars, 2) evaluate the pyrolysis temperature and steam activation on textural, surface and structural properties of biochars, 3) evaluate the effect of biochar properties on CO_2 adsorption, and 4) evaluate the adsorbents under more realistic dynamic flow conditions for the selective CO_2 adsorption from representative flue gas composition. Two contrastingly different feedstocks of paper mill sludge and pine sawdust were used to produce biochars at different pyrolysis temperatures and steam activation. These materials were screened for single component equilibrium CO_2 adsorption with a volumetric sorption analyzer. The materials with superior CO_2 capacity were then evaluated under the more relevant dynamic conditions with a representative flue gas composition of 15% CO_2 balanced by N_2.

2. Materials and methods

2.1. Biochar production and characterization

Biochars were produced from paper mill sludge and pine sawdust by slow pyrolysis. Feedstocks were dried at 60 °C and ground to <2 mm, and pyrolyzed in a muffle furnace (LT, Nabertherm, Germany) in covered ceramic crucibles at a heating rate of 7 °C min^{-1} for 2 h with no supply of air. Two different peak temperatures were used for pyrolyzing paper mill sludge, i.e., 300 and 600 °C, and it was 550 °C for pine sawdust. Biochar production temperatures were selected based on thermal gravimetric analysis of feedstocks in our previous studies (Lee et al., 2017; Lou et al., 2016). Steam-activated biochar was also produced from pine sawdust at 550 °C by purging steam at 5 mL min^{-1} to the specially designed pyrolyzing chamber for 45 min at 550 °C after completing the carbonization at 550 °C for 2 h. Total four biochars were produced, i.e., PMS300, PMS600, PS550 and PSS550. The abbreviations PMS, PS and PSS represent the paper mill sludge, pine sawdust and pine sawdust steam-activated, respectively.

Specific surface area of biochars was calculated by Brunauer–Emmett–Teller (BET) equation with N_2 adsorption-desorption isotherms at −196 °C obtained from a volumetric sorption analyzer (ASAP2020, Micromeritics). Biochars were further characterized for total pore volume, average pore diameter and average pore width with the same N_2 adsorption-desorption isotherm data. Raman spectroscopic (LabRam ARAMIS IR2, HORIBA JOBIN YVON) analysis and X-ray photoelectron spectroscopic (XPS, X-TOOL, ULVAC-PHI) analysis were done to determine the structural arrangements and surface functional groups of biochars respectively.

2.2. CO_2 adsorption

The CO_2 adsorption of biochars was determined by a volumetric sorption analyzer (ASAP2020, Micomeritics) at 25 °C. Before the CO_2 adsorption experiment biochar was degassed at 150 °C for 12 h under vacuum. Adsorption kinetics of CO_2 on selected biochars were tested by a thermogravimetric analyzer (TGA, Q50, TA instruments) at 30 °C.

2.3. Breakthrough experiments

Dynamic column breakthrough of mixture CO_2-N_2 measurements were conducted to evaluate the gas separation performance of our biochar adsorbents using our in-house built rig (Fig. 1). The biochar adsorbents were first sieved through ASTM No 35 sieve to obtain particles of similar size. Appropriately 1.2 g of adsorbent was loaded in the column (length = 214 mm, I.D. = 7 mm, Volume = 8.2 cm^3) which occupied a bed height of 45 mm and volume of 1.73 cm^3. The remaining column volume was filled by glass beads of 3 mm diameter previously washed and then dried overnight at 130 °C. Each of the sample was then degassed under flowing argon (Ar) at 150 °C for 6 h to ensure the complete removal of any volatile impurities adsorbed on the surfaces. The flow rate of Ar was maintained at 20 sccm using MFC (Alicat, US) and the ramp rate for attaining the target degassing temperature was 2 °C min^{-1}. After the degassing the adsorbent was cooled down to room temperature under Ar flow. The breakthrough experiments were then carried out at room temperature (23 ± 2 °C) and ambient atmospheric pressure. The Ar flow was switched to 8.5 sccm of N_2 (99.99% HKO Linde) and 1.5 sccm of CO_2 (99.95% HKO Linde) using the respective MFCs (Fig. 1). The concentration of the gases coming out of the column was monitored using an online mass spectrometry-based analyzer (Stanford Research Systems UGA300) till the detected gas concentration was the same to the initial mixture gas. The breakthrough experiments were corrected for gas analyzer response and dead space time by subtracting the blank capacity

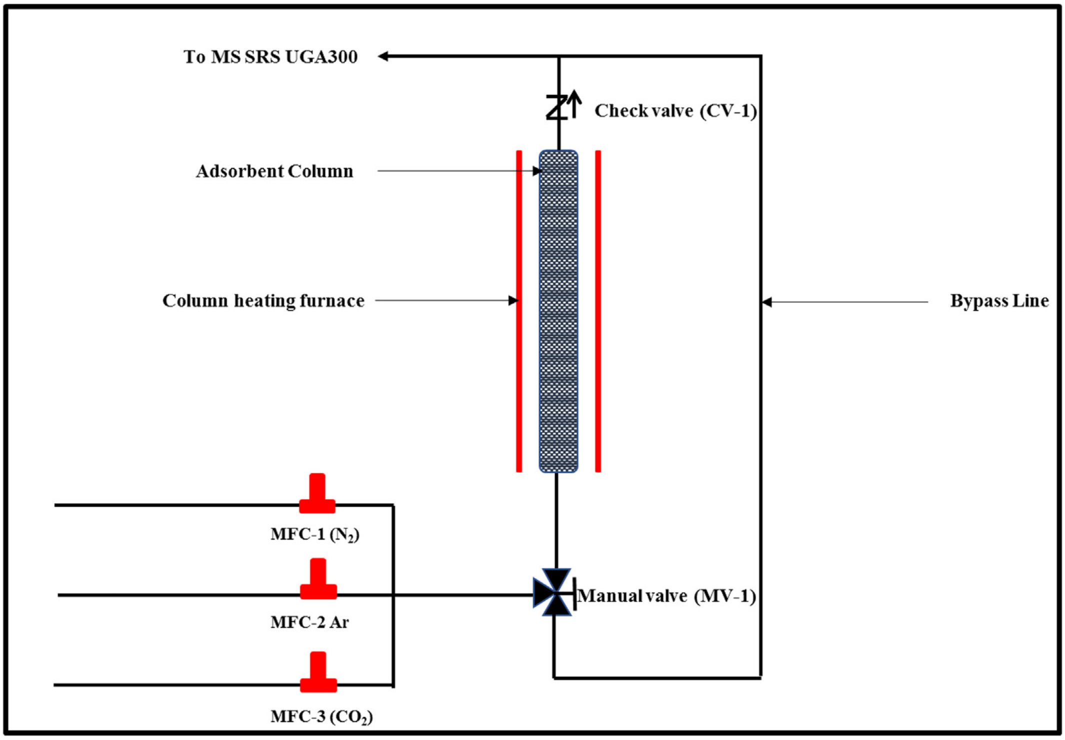

Fig. 1. Schematic of rig used for CO_2-N_2 dynamic breakthrough experiments. MFC denotes Mass Flow Controller.

obtained under similar conditions using glass beads only. The specific breakthrough capacities of adsorbent column for different gases were calculated using the following equation,

$$X_{BT} = \frac{F_r}{22.4w}\left(\int_0^{t_s}(C_0-C)dt - \int_0^{t_b}(C_0-C)dt\right) \tag{1}$$

where χ_{BT} is specific breakthrough capacity of adsorbent in mmol/g for a particular gas component in the mixture.

t_s is breakthrough time (when $C=C_0$) in minutes when adsorbent is loaded.

t_b is breakthrough time in minutes for blank experiment.

F_r is total flow rate of the gas component in sccm.

w is weight of adsorbent after activation in gram.

C_0 is concentration of component in feed.

C is outlet concentration at time t.

The selectivity of the adsorbent was calculated from the breakthrough capacities of the adsorbents for different gases using the formula (Durán et al., 2018).

$$S_{CO_2/N_2} = \left(\frac{X_{BT(CO_2)}}{X_{BT(N_2)}}\right)\left(\frac{p_{N_2}}{p_{co_2}}\right) \tag{2}$$

3. Results and discussion

3.1. Biochar textural properties

The N_2 adsorption of four biochars were positively correlated to their S_{BET} (Pearson correlation coefficient $(r) = 0.9111$, $p = 0.0889$), PSS550 which showed the highest S_{BET} had the highest N_2 adsorption and lowest N_2 adsorption was showed in the PMS300 which had the lowest S_{BET} (Fig. 2a). The two biochars produced from pine sawdust showed higher specific surface area (S_{BET}) than the biochars produced from paper mill sludge (Table 1). The inherent porous structures of woody feedstocks could be the reason for the considerably high S_{BET} of PS550 and PSS550 (Cao et al., 2018). Steam activation of PS550 showed a noticeable increase in S_{BET} of PSS550. This is likely due to the generation of micropores as observed from the pore size distribution (Fig. 2). Shim et al. (2015) also reported increased surface area in biochar after steam activation due to the development of micropores.

Pore size distribution of four biochars showed dissimilar patterns to each other (Fig. 2b). The PMS300 showed the highest amount of pores with a size of 0.35–0.5 nm and followed by 1.2–2 nm size pores. Similar to the PMS300, PMS600 also had the highest amount of pores with a size of 0.35–0.5 nm, and followed by pores with a size of 1.3–2 nm. Moreover, PMS600 had considerable amount of large size pores i.e., 3–20 nm. The high pyrolysis temperature of PMS600 might have created new micropores and large size pores due to removal of volatile matter in biochar (Igalavithana et al., 2017b). It is further confirmed from the comparatively lower average pore diameter (i.e., PMS300: 17.16 nm and PMS600: 11.27 nm) and average pore width (i.e., PMS300: 9.28 nm and PMS600: 8.93 nm) of PMS600 compared to the PMS300 (Table 1). Moreover, PMS600 had higher pore volume at each pore width of 0.2–20 nm than PMS300 (Fig. 2c). The pore size distribution of PS550 and PSS550 is different from that of paper mill sludge biochars and they consist of very small size pores (Fig. 2b). The PS500 had the highest amount of 0.4–0.8 nm size pores and those of PSS550 were 0.4–0.5 nm. Hence, PSS500 had very small size pores compared to the PS550, and average pore diameter and average pore width of PSS550 (i.e., average pore diameter: 2.24 nm and average pore width: 2.06 nm) were lower than those of the PS550 (i.e., average pore diameter: 2.86 nm and average pore width: 2.18 nm) and paper mill sludge biochars (Table 1). Both PS550 and PSS550 had a negligible amount of pores having width of >2 nm, and they had relatively large volume of small size pores compared to the paper mill sludge biochars (Fig. 2c). Moreover, PSS550 had the highest amount of small pores (i.e., pore width <1 nm) from four biochars. It is obvious that steam activation of PSS550 favourably produced micro pores in its structure. Moreover PSS550 showed the highest volume of 0.5 nm size micropores which is the most favourable for CO_2 adsorption (Wei et al., 2012).

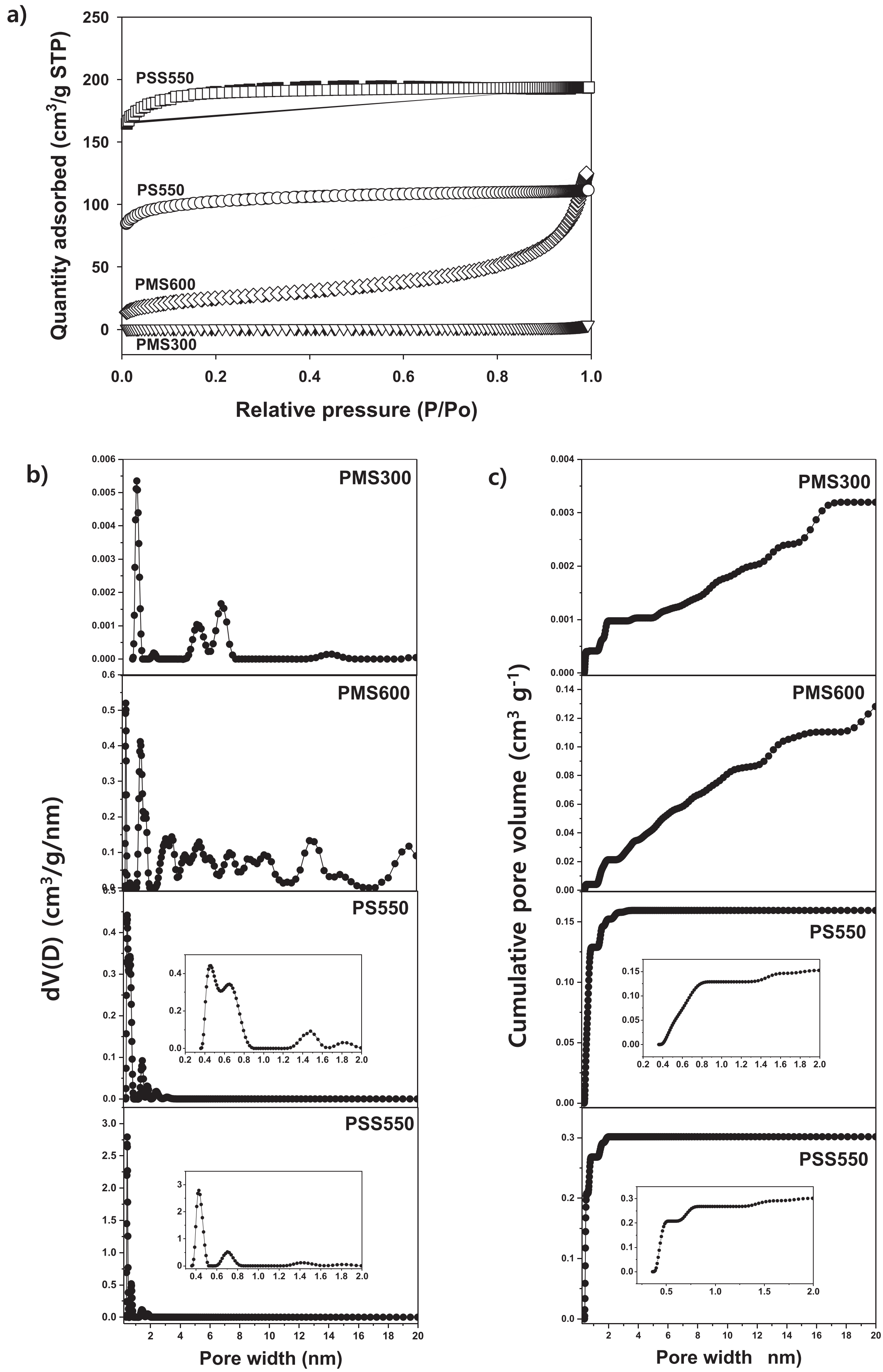

Fig. 2. a) N_2 adsorption-desorption isotherms at −196 °C, b) pore size distribution and c) cumulative pore volume of biochars determined by density functional theory.

Table 1
Textural properties of biochars.

Biochar	S_{BET}[a]	V_T[a]	Average pore diameter[a]	Average pore width[a]
	$m^2\ g^{-1}$	$cm^3 g^{-1}$	nm	nm
PMS300	53.83	0.11	17.16	9.28
PMS600	86.43	0.17	11.27	8.93
PS550	315.59	0.17	2.86	2.18
PSS550	581.74	0.25	2.24	2.06

S_{BET}; Specific surface area calculated by the BET method.
V_T: Total pore volume at P/P_0 of ~0.99.
[a] Calculated by using Barrett-Joyner-Halenda (BJH) method from N_2 adsorption data.

Table 2
XPS derived elemental composition (atomic %) of biochar surface.

Biochar	Pyrolysis temperature	C1s	O1s	N1s	S2p
	°C	%	%	%	%
PMS300	300	66.46	30.29	2.31	0.93
PMS600	600	67.79	30.49	0.80	0.92
PS550	550	89.98	9.16	0.75	0.10
PSS550	550	88.23	11.05	0.57	0.15

3.2. XPS analysis

The C% on biochar surface was higher in pine sawdust biochars than the paper mill sludge biochars (Table 2). Contrariwise, the O% was higher in paper mill sludge biochars than the pine sawdust biochars. Similarly, Enders et al. (2012) reported high C% and low O% in woody biochar and inversely in paper mill sludge biochar. Authors have explained this as high ash content in paper mill sludge increases the O% in that biochar. The surface C% in PMS600 slightly increased compared to the PMS300 with respect to the high pyrolysis temperature of PMS600 (Igalavithana et al., 2017a). However, the O% did not show any significant change. The N% in the surface of PMS600 noticeably decreased in PMS600 compared to the PMS300. The high pyrolysis temperature of PMS600 compared to the PMS300 might decrease the surface N% due to its temperature sensitivity (Igalavithana et al., 2017b). The steam activation of pine sawdust biochar (i.e., PSS550) increased the O% and decreased the C% on PSS550 surface. This might be due to the removal of volatile matter and oxidation of biochar surface caused by the steam activation (Rajapaksha et al., 2016a, 2016b). Moreover, the steam activation of PSS550 showed considerable decrease in surface N% compared to the PS550. Rajapaksha et al. (2015) also observed decreased N% in steam activated biochar produced from burcucumber at 700 °C compared to the non-steam activated biochar produced under similar conditions. However, there was no difference in N% in steam activated and non-steam activated burcucumber

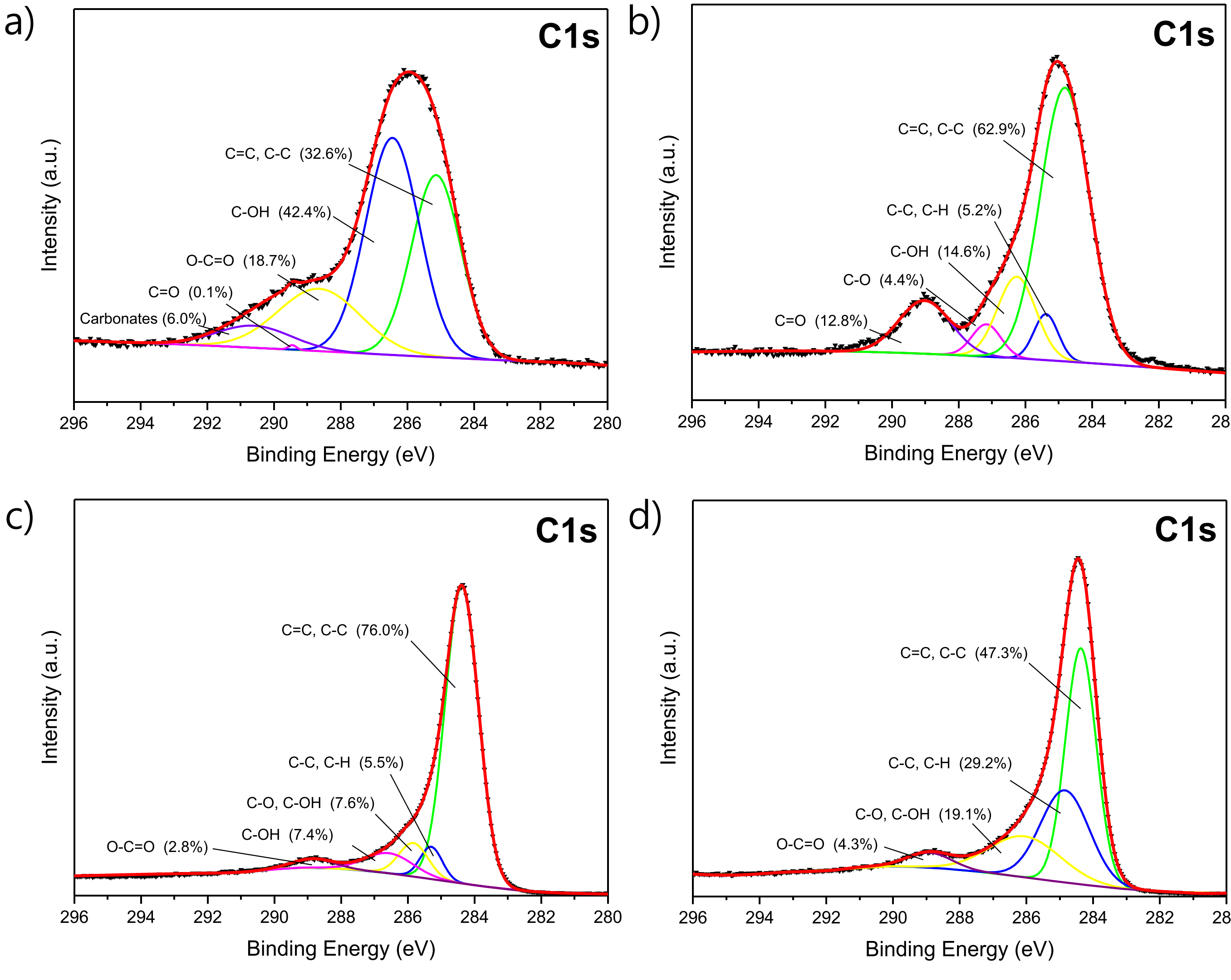

Fig. 3. XPS C1s deconvolution spectra a) PMS300, b) PMS 600, c) PS550, d) PSS550.

biochars produced at 300 °C. Surface S% did not show considerable change depending on the pyrolysis temperature or steam activation in paper mill sludge biochar and pine sawdust biochar respectively.

The C1s peak of PMS300 and PMS600 was deconvoluted into five peaks, and representing aromatic C=C and aliphatic C—C (285.1–285.4 eV) and C—OH (286.3–286.4 eV) were common to both biochars (Fig. 3a and b) (Min et al., 2016). In PMS300 and PMS600 the dominant functional group was aromatic C=C and aliphatic C—C, and its proportion was increased in PMS600 (i.e., 62.9%) compared to the PMS300 (i.e., 32.6%). This might be due to the increase of aromatic carbon structures in PMS600 due to higher carbonization than PMS300 at relatively high pyrolysis temperature (Igalavithana et al., 2017a). The proportion of oxygen containing functional groups of C—OH (286.4–287.1 eV) (i.e., 14.6%) was reduced in PMS600 compared to the PMS300 (i.e., 42.4%). Moreover, two functional groups of PMS300, i.e., O—C=O (288.6 eV) and carbonates (290.6 eV) disappeared in PMS600. The high pyrolysis temperature was the reason for the reduced amount of oxygen containing functional groups in PMS600 (Ahmad et al., 2014; Igalavithana et al., 2017a, 2017b). In PS550 and PSS550, aromatic C=C and aliphatic C—C (284.4 eV) are also the dominant functional groups, and its deceased proportion in PSS550 compared to the PS550 may be due to the removal of aliphatic carbons or volatile matter from biochar matrix during the steam activation (Fig. 3c and d) (Kołtowski et al., 2016; Sizmur et al., 2017). Even though the proportion of the functional group of aliphatic C—C and C—H (284.8–285.3 eV) was increased in PSS550 (i.e., 29.2%) than the PS550 (i.e., 5.5%), the total of aromatic C=C and aliphatic C—C, and aliphatic C—C and C—H in PSS550 (i.e., 76.5%) was lower than that of the PS550 (i.e., 81.5%). Hence, it is apparent that steam activation reduced the volatile carbons in PSS550. Moreover, steam activation increased the proportions of oxygen containing functional groups in PSS550 (i.e., C—O and C—OH, 258.8–286.0 eV and O—C=O, 288.8–288.9 eV) as explained above.

3.3. Raman analysis

Several bands were obtained in the curve fitting of Raman spectra of four biochars (Fig. 4). The D band of Raman spectrum represents the highly ordered defect large aromatic ring structures which contain not less than six fused rings and G band represents the bond stretching of pairs of sp^2 atoms in carbon ring and chain structures (Igalavithana et al., 2017c; Yang et al., 2018). The ratios of integrated intensity (peak area (A)) of D and G bands (i.e., A_D/A_G) denote the defect structures to ordered structures in biochar (Gustavo Cançado et al., 2017; Quosai et al., 2018). Lower values of A_D/A_G ratio of biochar describe the presence of higher amount of ordered carbon structures (Wei et al., 2016). The A_D/A_G ratio of PMS300 was 7.92 and that of PMS600 was 2.21. Hence, it is apparent that high pyrolysis temperature of PMS600 increased the aromatic carbon structures compared to the

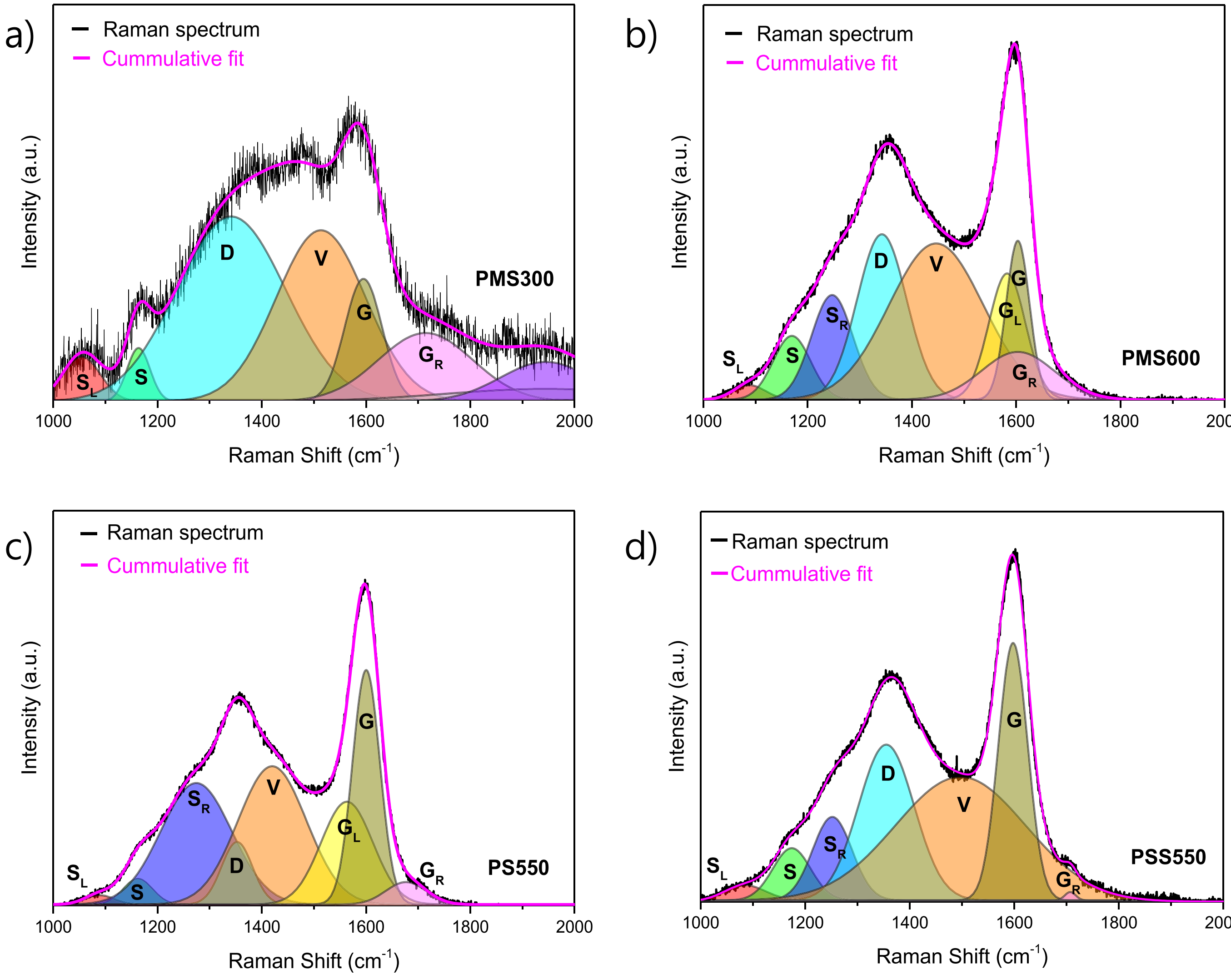

Fig. 4. Curve fitting of Raman spectra a) PMS300, b) PMS 600, c) PS550 and d) PSS550.

PMS300. The A_D/A_G ratio of PS550 (i.e., 0.30) was lower than that of the PSS550 (i.e., 1.15), implying that PS550 contained more amount of ordered carbon structures. However, these values appeared due to the low area of D band and high area of G band of PS550 than the PSS550. Hence, the amount of highly ordered defect large aromatic ring structures is high in PSS550 compared to the PS550.

The group of S_L, S and S_R bands represent the aryl-alkyl ether, para-aromatics, C(aromatic)C—(alkyl), C—H in aromatic rings and sp^3 of hexagonal diamond carbon (Feng et al., 2016; Maliutina et al., 2018). The two bands of V and G_L represent the amorphous carbon structures and aromatic carbon structures consisting with few aromatic rings (Pusceddu et al., 2016). The presence of G_L band in PMS600 compared to the PMS300 may be due to the breakdown of large aromatic ring structures due to the high pyrolysis temperature. The absence of G_L band in PSS550 compared to the PS550 might be due to the removal of amorphous carbon structures or volatile matter during the steam activation (Rajapaksha et al., 2016b).

3.4. CO_2 adsorption on biochars

The highest CO_2 adsorption was showed by PSS550 at 1 bar and 25 °C, and slightly lower adsorption was illustrated by PS550 (Fig. 5a). The CO_2 adsorption of paper mill sludge biochars was significantly lower than that of the pine sawdust biochars, and PMS600 showed slightly higher CO_2 adsorption than PMS300. The noticeably higher CO_2 adsorption by PS550 and PSS550 might be due to the highest surface area of these two biochars than paper mill sludge biochars, hence, physisorption might be the principal mechanism of CO_2 adsorption on biochars (Hong et al., 2016; Shafeeyan et al., 2011; Zhang et al., 2014). Moreover, a considerably high amount of micropores with 0.3–0.8 nm diameter was observed in pine sawdust biochars than in paper mill sludge biochars. Pearson correlation analysis of CO_2 adsorption and pore volume of micropores of 0.3–0.8 nm showed significant positive correlation ($r = 0.862$, $p = 0.138$). These micropores are known to be favourable for the CO_2 adsorption (Klasson et al., 2015; Wei et al., 2012). Micropore volume of 0.5 nm size is the most effective for CO_2 adsorption and those pores were the highest in PSS550 as explained in Section 3.1, and 0.5 nm size micropores was shown very strong positive correlation to the CO_2 adsorption ($r = 0.960$, $p = 0.039$).

Two paper mill sludge biochars showed high amount of oxygen containing acidic functional groups (i.e., C—OH and O—C=O) than the PS550 and PSS550 as observed from the XPS analysis, hence the surface of PMS300 and PMS600 is likely to be acidic, which is not encouraging the CO_2 adsorption (Shafeeyan et al., 2010). Even though PSS550 showed considerably higher S_{BET} than PS550, the CO_2 adsorption of these two biochars did not show substantial difference. This might be due to the comparatively high N containing functional groups on PS550 than PSS550. Similarly, Creamer et al. (2014) observed higher CO_2 adsorption on a biochar having high N% on its surface than a biochar having high surface area. As authors explained the presence of high amount of N-containing functional groups have promoted the physisorption of CO_2 on biochar surfaces due to strong interaction among acidic CO_2 (Lewis acid) and basic N-containing functional groups. In addition, the higher aromatic structures presence in pine sawdust biochars than the paper mill sludge biochars, as revealed from Raman analysis, might have increased the van der Waals forces between biochar matrix and CO_2 to increase the physisorption of CO_2 on PS550 and PSS550 (Shafeeyan et al., 2011). Furthermore, pine sawdust biochars showed relatively higher CO_2 adsorption (PS550: 1.66 mol kg^{-1}, PSS550: 1.76 mol kg^{-1}) compared to the biochars in studies conducted under similar experimental conditions (see supplementary materials of (Dissanayake et al., 2020a)), also it showed comparable CO_2 adsorption to other adsorbents (see Supplementary materials of (Igalavithana et al., 2019)). The CO_2 adsorption of pine sawdust biochar could be further increased by impregnation of alkali and alkali earth metals (Xu et al., 2016), and KOH activation (Igalavithana et al., 2019) which needs to be evaluated compared to the commercial materials in future studies.

Adsorption kinetics of CO_2 onto PS550 was tested as a representative sample since steam activation did not show significant improvement in CO_2 adsorption of PSS550 (Fig. 5b). Adsorption of CO_2 was rapid at the start, showed reduced speed after about 5 min, and came to a plateau after about 90 min, representing it was at equilibrium.

The CO_2 adsorption isotherms of biochars were fitted to Langmuir and Freundlich models (Fig. 5a and Table 3). All isotherms except PSS550 were best fitted to Freundlich model with the correlation coefficients of >0.995. The PSS550 was best fitted to Langmuir model with a correlation coefficient of >0.996. Hence, CO_2 adsorption on PMS300, PMS600 and PS550 could be a multilayer adsorption and it may be a monolayer adsorption on PSS550 (Vilarrasa-García et al., 2015). However, as both Freundlich and Langmuir models were fitted with correlation coefficients of >0.99, the CO_2 adsorption of four biochars can be described as multilayer or monolayer. The magnitude of the Freundlich empirical constant (n) <1 indicates the affinity of biochar surfaces for adsorption. The n value of all biochars were < 1 representing the favourable CO_2 adsorption on biochar surfaces (Khalili et al., 2015; Rajapaksha et al., 2015).

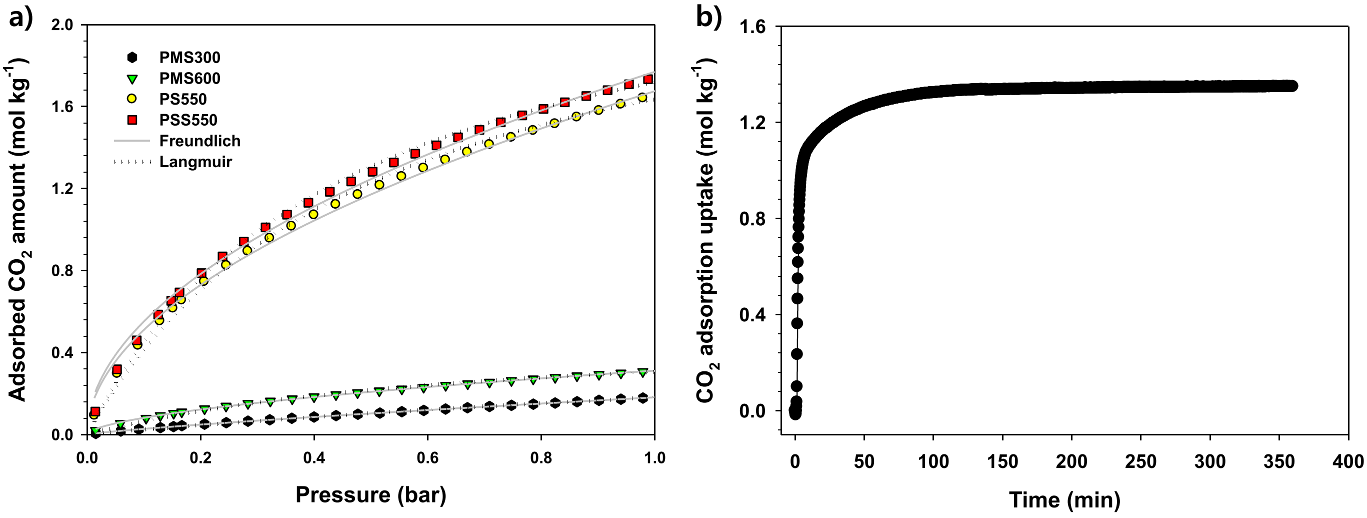

Fig. 5. a) CO_2 adsorption isotherms at 25 °C and b) adsorption kinetics of CO_2 onto PS550 at 30 °C.

Table 3
Langmuir and Freundlich adsorption isotherm model parameters for the CO_2 adsorption on biochars.

Biochar	Freundlich			Langmuir		
	$q = K_F P_{CO2}^{1/n}$			$q = q_{max} K_L P_{CO2}/(1 + K_L P_{CO2})$		
	K_F	n	r^2	q_{max}	K_L	r^2
	mol $kg^{(-1)}$ $atm^{(-1/n)}$			mol kg^{-1}	L $atm^{(-1)}$	
PMS300	0.181	0.819	0.99992	0.694	0.352	0.99830
PMS600	0.312	0.582	0.99939	0.523	1.414	0.99251
PS550	1.675	0.516	0.99588	2.440	2.031	0.99480
PSS550	1.769	0.506	0.99425	2.498	2.201	0.99611

P_{CO2}: CO_2 partial pressure.
q_{max}: amount of CO_2 adsorbed with monolayer coverage.
K_L: Langmuir constant.
K_F: Freundlich constant.
n: Freundlich empirical constant.

3.5. Gas separation

Breakthrough adsorption measurements are better representatives of the practical gas separation applications where adsorption always takes place from the mixture of gases under dynamic flow conditions. Unlike pure component static isotherms, the dynamic adsorption gives a realistic picture of separation performance of the adsorbents taking into consideration of the kinetic as well as thermodynamic aspects of adsorption. The breakthrough curves for the investigated adsorbents are shown in Fig. 6. Capacities of CO_2, N_2 and CO_2 over N_2 selectivity of the adsorbents calculated from the breakthrough curves are presented in Table 4. It is evident following the steam activation though there is slight increase in CO_2 capacity from 0.67 mmol/g to 0.73 mmol/g the improvement in CO_2 over N_2 selectivity is significant from 18.28 for PS550 to 26.70 for PSS550. These selectivities of 18.28 and 26.70 correspond to 76% and 83% CO_2 stream purity, respectively, during desorption (Fayemiwo et al., 2018). The improved CO_2 over N_2 selectivity of PSS550 than PS550 can be attributed to its narrow micropore size

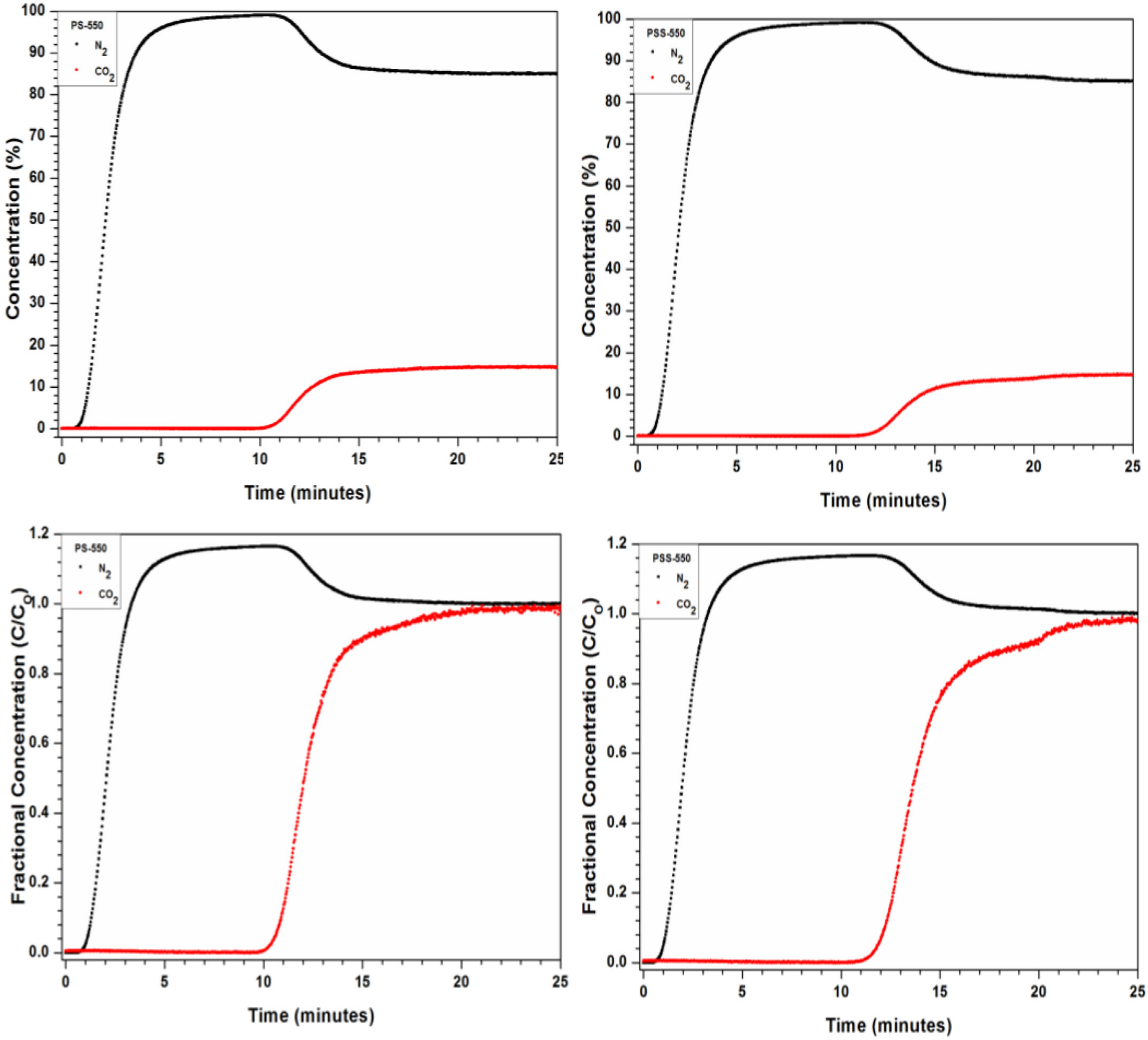

Fig. 6. CO_2 and N_2 breakthrough curves of PS550 and PSS550. Feed concentration 15% CO_2 and N_2, Total feed flow 10 sccm, Temperature 23 ± 2 °C, Total Pressure = 1.01 bar.

Table 4
Saturation breakthrough capacities and selectivity of adsorbents.

Adsorbent	Weight for analysis	N_2 capacity	CO_2 capacity	$S_{CO2/N2}$
	g	mmol g^{-1}	mmol g^{-1}	
PS550	1.03939	0.21	0.67	18.28
PSS550	1.1124	0.15	0.73	26.70

distribution centered around 0.35–0.5 nm (Fig. 2). During the dynamic adsorption studies CO_2 molecules with smaller kinetic diameter of 0.33 nm (Mehio et al., 2014; Yang et al., 2012) can easily enter these pores and get adsorbed whereas relatively larger N_2 molecules with kinetic diameter of 0.36 nm (Mehio et al., 2014; Yang et al., 2012) face diffusion constraints to be admitted into these pores thus limiting their adsorption. In fact, the pore diameter of our PSS550 samples has been suggested as the most suitable pore size for efficient CO_2 adsorption (Wei et al., 2012). Moreover, as confirmed by XPS, the higher proportion of oxygen containing functional groups (C—O, a basic functional group) in PSS550 could lead to stronger electrostatic or hydrogen bonding interaction with CO_2 thereby improving CO_2 over N_2 selectivity (Liu et al., 2018). Thus in general the carbon materials with narrow and very small micropore size distribution and oxygen functionalities such as carbonyl and hydroxyl groups can be a better adsorbent for selective CO_2 sorption under dynamic conditions.

4. Conclusion

Biochar produced from pine sawdust possesses a higher potential to adsorb CO_2 than the paper mill sludge biochars. Comparatively high surface area and micro porous structures of pine sawdust biochar might be the main reasons for the significantly high CO_2 adsorption by pine sawdust biochars. Also, the high aromaticity of pine sawdust biochars over the paper mill sludge biochars might have facilitated the CO_2 adsorption by increasing van der Waals forces between the biochar matrix and CO_2. Moreover, the steam activated biochar (i.e., PSS550) had somewhat higher CO_2 adsorption capacity and CO_2 selectivity over N_2 than the biochar without steam activation (i.e., PS550). High surface area, microporosity and comparatively high O containing basic functional groups compared to the PS550 could be responsible for the improved CO_2 adsorption performance of PSS550. However, the slight difference in CO_2 adsorption of two pine sawdust biochars might be due to the higher N containing functional groups on PS500 than PSS550, which provide basic nature to the biochar surface. The paper mill sludge biochar produced at high temperature (i.e., PMS600) showed comparatively high CO_2 adsorption than that produced at low temperature (i.e., PMS300). Development of more micropores and increased surface area at high pyrolysis temperature might be the main reason for that. Results clearly indicate that pine sawdust biochar is a suitable low cost and sustainable adsorbent for CO_2 at 25 °C; hence, it can be effectively developed to use to adsorb CO_2 at industrial sites. Further studies are required to evaluate the modified pine sawdust biochar produced to increase the surface N-containing functional groups, alkali and alkali earth metals, and microporosity for CO_2 adsorption.

CRediT authorship contribution statement

Avanthi Deshani Igalavithana: Formal analysis, Writing - original draft. **Seung Wan Choi:** Formal analysis, Writing - original draft. **Jin Shang:** Writing - review & editing. **Aamir Hanif:** Formal analysis, Writing - original draft. **Pavani Dulanja Dissanayake:** Formal analysis. **Daniel C.W. Tsang:** Writing - review & editing. **Jung-Hwan Kwon:** Writing - review & editing. **Ki Bong Lee:** Conceptualization, Funding acquisition, Supervision, Writing - review & editing. **Yong Sik Ok:** Conceptualization, Funding acquisition, Supervision, Writing - review & editing.

Declaration of competing interest

The authors declare that they have no known competing financial interests or personal relationships that could have appeared to influence the work reported in this paper.

Acknowledgement

This study was supported by the Public Technology Program based on Environment Policy (E416-00070-0604-0) funded by the Korean Ministry of Environment (MOE), a National Research Foundation (NRF) grant funded by the Korean Ministry of Education through the Basic Science Research Program (NRF-2018R1D1A1B07050321) and the Korea Ministry of Environment (MOE) as “Technology Program for establishing biocide safety management” (2018002490001). Authors also wish to acknowledge Jae Hoon Park at Korea University for supporting to conduct a part of this study in the City University of Hong Kong.

References

Ahmad, M., Rajapaksha, A.U., Lim, J.E., Zhang, M., Bolan, N., Mohan, D., Vithanage, M., Lee, S.S., Ok, Y.S., 2014. Biochar as a sorbent for contaminant management in soil and water: a review. Chemosphere 99, 19–33. https://doi.org/10.1016/j.chemosphere.2013.10.071.

Cao, L., Yu, I.K.M., Tsang, D.C.W., Zhang, S., Ok, Y.S., Kwon, E.E., Song, H., Poon, C.S., 2018. Phosphoric acid-activated wood biochar for catalytic conversion of starch-rich food waste into glucose and 5-hydroxymethylfurfural. Bioresour. Technol. 267, 242–248. https://doi.org/10.1016/J.BIORTECH.2018.07.048.

Choi, S.W., Tang, J., Pol, V.G., Lee, K.B., 2019. Pollen-derived porous carbon by KOH activation: effect of physicochemical structure on CO_2 adsorption. J. CO_2 Util. 29, 146–155. https://doi.org/10.1016/J.JCOU.2018.12.005.

Creamer, A.E., Gao, B., Zhang, M., 2014. Carbon dioxide capture using biochar produced from sugarcane bagasse and hickory wood. Chem. Eng. J. 249, 174–179. https://doi.org/10.1016/J.CEJ.2014.03.105.

Dissanayake, P.D., Choi, S.W., Igalavithana, A.D., Yang, X., Tsang, D.C.W., Wang, C.H., Kua, H.W., Lee, K.B., Ok, Y.S., 2020a. Sustainable gasification biochar as a high efficiency adsorbent for CO_2 capture: a facile method to designer biochar fabrication. Renew. Sust. Energ. Rev. 124, 109785. https://doi.org/10.1016/j.rser.2020.109785.

Dissanayake, P.D., You, S., Igalavithana, A.D., Xia, Y., Bhatnagar, A., Gupta, S., Kua, H.W., Kim, S., Kwon, J.H., Tsang, D.C.W., Ok, Y.S., 2020b. Biochar-based adsorbents for carbon dioxide capture: a critical review. Renew. Sust. Energ. Rev. https://doi.org/10.1016/j.rser.2019.109582.

Durán, I., Álvarez-Gutiérrez, N., Rubiera, F., Pevida, C., 2018. Biogas purification by means of adsorption on pine sawdust-based activated carbon: impact of water vapor. Chem. Eng. J. 353, 197–207. https://doi.org/10.1016/J.CEJ.2018.07.100.

Enders, A., Hanley, K., Whitman, T., Joseph, S., Lehmann, J., 2012. Characterization of biochars to evaluate recalcitrance and agronomic performance. Bioresour. Technol. 114, 644–653. https://doi.org/10.1016/j.biortech.2012.03.022.

Fayemiwo, K.A., Vladisavljević, G.T., Nabavi, S.A., Benyahia, B., Hanak, D.P., Loponov, K.N., Manović, V., 2018. Nitrogen-rich hyper-crosslinked polymers for low-pressure CO_2 capture. Chem. Eng. J. 334, 2004–2013. https://doi.org/10.1016/J.CEJ.2017.11.106.

Feng, D., Zhao, Y., Zhang, Y., Sun, S., Meng, S., Guo, Y., Huang, Y., 2016. Effects of K and Ca on reforming of model tar compounds with pyrolysis biochars under H_2O or CO_2. Chem. Eng. J. 306, 422–432. https://doi.org/10.1016/J.CEJ.2016.07.065.

Franchi, R.S., Harlick, P.J.E., Sayari, A., 2005. Applications of Pore-expanded Mesoporous Silica. 2. Development of a High-capacity, Water-tolerant Adsorbent for CO2. https://doi.org/10.1021/IE0504194.

Gargiulo, V., Gomis-Berenguer, A., Giudicianni, P., Ania, C.O., Ragucci, R., Alfè, M., 2018. Assessing the potential of biochars prepared by steam-assisted slow pyrolysis for CO_2 adsorption and separation. Energy Fuel 32, 10218–10227. https://doi.org/10.1021/acs.energyfuels.8b01058.

Gustavo Cançado, L., Gomes da Silva, M., Martins Ferreira, E.H., Hof, F., Kampioti, K., Huang, K., Pénicaud, A., Alberto Achete, C., Capaz, R.B., Jorio, A., 2017. Disentangling contributions of point and line defects in the Raman spectra of graphene-related materials. 2D Mater 4, 025039. https://doi.org/10.1088/2053-1583/aa5e77.

Hanif, A., Dasgupta, S., Nanoti, A., 2016. Facile synthesis of high-surface-area mesoporous MgO with excellent high-temperature CO_2 adsorption potential. Ind. Eng. Chem. Res. 55, 8070–8078. https://doi.org/10.1021/acs.iecr.6b00647.

Hanif, A., Sun, M., Shang, S., Tian, Y., Yip, A.C.K., Ok, Y.S., Yu, I.K.M., Tsang, D.C.W., Gu, Q., Shang, J., 2019. Exfoliated Ni-Al LDH 2D nanosheets for intermediate temperature CO_2 capture. J. Hazard. Mater. 374, 365–371. https://doi.org/10.1016/J.JHAZMAT.2019.04.049.

Hansen, K., Mathiesen, B.V., Skov, I.R., 2019. Full energy system transition towards 100% renewable energy in Germany in 2050. Renew. Sust. Energ. Rev. 102, 1–13. https://doi.org/10.1016/J.RSER.2018.11.038.

Hong, S.-M., Jang, E., Dysart, A.D., Pol, V.G., Lee, K.B., 2016. CO_2 capture in the sustainable wheat-derived activated microporous carbon compartments. Sci. Rep. 6, 34590. https://doi.org/10.1038/srep34590.

Igalavithana, A.D., Lee, S.E., Lee, Y.H., Tsang, D.C.W., Rinklebe, J., Kwon, E.E., Ok, Y.S., 2017a. Heavy metal immobilization and microbial community abundance by vegetable waste and pine cone biochar of agricultural soils. Chemosphere 174, 593–603. https://doi.org/10.1016/j.chemosphere.2017.01.148.

Igalavithana, A.D., Mandal, S., Niazi, N.K., Vithanage, M., Parikh, S.J., Mukome, F.N.D., Rizwan, M., Oleszczuk, P., Al-Wabel, M., Bolan, N., Tsang, D.C.W., Kim, K.-H., Ok, Y.S., 2017b. Advances and future directions of biochar characterization methods and applications. Crit. Rev. Environ. Sci. Technol. 47, 2275–2330. https://doi.org/10.1080/10643389.2017.1421844.

Igalavithana, A.D., Park, J., Ryu, C., Lee, Y.H., Hashimoto, Y., Huang, L., Kwon, E.E., Ok, Y.S., Lee, S.S., 2017c. Slow pyrolyzed biochars from crop residues for soil metal(loid) immobilization and microbial community abundance in contaminated agricultural soils. Chemosphere 177, 157–166. https://doi.org/10.1016/j.chemosphere.2017.02.112.

Igalavithana, A.D., Yang, X., Zahra, H.R., Tack, F.M.G., Tsang, D.C.W., Kwon, E.E., Ok, Y.S., 2018. Metal(loid) immobilization in soils with biochars pyrolyzed in N_2 and CO_2 environments. Sci. Total Environ. 630. https://doi.org/10.1016/j.scitotenv.2018.02.185.

Igalavithana, A.D., Wan Choi, S., Dissanayake, P.D., Shang, J., Wang, C.-H., Yang, X., Kim, S., Tsang, D.C.W., Lee, K.B., Ok, Y.S., 2019. Gasification biochar from biowaste (food waste and wood waste) for effective CO2 adsorption. J. Hazard. Mater., 121147 https://doi.org/10.1016/J.JHAZMAT.2019.121147.

Jeon, S., Jung, H., Kim, S.H., Lee, K.B., 2018. Double-layer structured CO_2 adsorbent functionalized with modified polyethyleneimine for high physical and chemical stability. ACS Appl. Mater. Interfaces 10, 21213–21223. https://doi.org/10.1021/acsami.8b01749.

Khalili, S., Khoshandam, B., Jahanshahi, M., 2015. Optimization of Production Conditions for Synthesis of Chemically Activated Carbon Produced From Pine Cone Using Response Surface Methodology for CO_2 Adsorption. https://doi.org/10.1039/c5ra18986a.

Klasson, K.T., Uchimiya, M., Lima, I.M., 2015. Characterization of narrow micropores in almond shell biochars by nitrogen, carbon dioxide, and hydrogen adsorption. Ind. Crop. Prod. 67, 33–40. https://doi.org/10.1016/J.INDCROP.2015.01.010.

Kloutse, F., Hourri, A., Natarajan, S., Benard, P., Chahine, R., 2018. Experimental benchmark data of CH4, CO2 and N2 binary and ternary mixtures adsorption on MOF-5. Sep. Purif. Technol. 197, 228–236. https://doi.org/10.1016/J.SEPPUR.2018.01.013.

Kołtowski, M., Hilber, I., Bucheli, T.D., Oleszczuk, P., 2016. Effect of steam activated biochar application to industrially contaminated soils on bioavailability of polycyclic aromatic hydrocarbons and ecotoxicity of soils. Sci. Total Environ. 566–567, 1023–1031. https://doi.org/10.1016/J.SCITOTENV.2016.05.114.

Kua, H.W., Pedapati, C., Lee, R.V., Kawi, S., 2019. Effect of indoor contamination on carbon dioxide adsorption of wood-based biochar – lessons for direct air capture. J. Clean. Prod. 210, 860–871. https://doi.org/10.1016/J.JCLEPRO.2018.10.206.

Lee, J., Tsang, Y.F., Kim, S., Ok, Y.S., Kwon, E.E., 2017. Energy density enhancement via pyrolysis of paper mill sludge using CO_2. J. CO_2 Util. 17, 305–311. https://doi.org/10.1016/j.jcou.2017.01.001.

Letcher, T.M., 2019. Why do we have global warming? Managing Global Warming. Elsevier, pp. 3–15. https://doi.org/10.1016/b978-0-12-814104-5.00001-6

Li, Y., Ruan, G., Jalilov, A.S., Tarkunde, Y.R., Fei, H., Tour, J.M., 2016. Biochar as a renewable source for high-performance CO_2 sorbent. Carbon N. Y. 107, 344–351. https://doi.org/10.1016/J.CARBON.2016.06.010.

Liu, B., Li, H., Ma, X., Chen, R., Wang, S., Li, L., 2018. The synergistic effect of oxygen-containing functional groups on CO_2 adsorption by the glucose–potassium citrate-derived activated carbon. RSC Adv. 8, 38965–38973. https://doi.org/10.1039/C8RA05523H.

Lou, K., Rajapaksha, A.U., Ok, Y.S., Chang, S.X., 2016. Pyrolysis temperature and steam activation effects on sorption of phosphate on pine sawdust biochars in aqueous solutions. Chem. Speciat. Bioavailab. 28, 42–50. https://doi.org/10.1080/09542299.2016.1165080.

Maliutina, K., Tahmasebi, A., Yu, J., 2018. Effects of pressure on morphology and structure of bio-char from pressurized entrained-flow pyrolysis of microalgae. Data Br 18, 422–431. https://doi.org/10.1016/J.DIB.2018.03.048.

Mandal, S., Sarkar, B., Igalavithana, A.D., Ok, Y.S., Yang, X., Lombi, E., Bolan, N., 2017. Mechanistic insights of 2,4-D sorption onto biochar: influence of feedstock materials and biochar properties. Bioresour. Technol. https://doi.org/10.1016/j.biortech.2017.07.073.

McDonald, T.M., Mason, J.A., Kong, X., Bloch, E.D., Gygi, D., Dani, A., Crocellà, V., Giordanino, F., Odoh, S.O., Drisdell, W.S., Vlaisavljevich, B., Dzubak, A.L., Poloni, R., Schnell, S.K., Planas, N., Lee, K., Pascal, T., Wan, L.F., Prendergast, D., Neaton, J.B., Smit, B., Kortright, J.B., Gagliardi, L., Bordiga, S., Reimer, J.A., Long, J.R., 2015. Cooperative insertion of CO2 in diamine-appended metal-organic frameworks. Nature 519, 303–308. https://doi.org/10.1038/nature14327.

Mehio, N., Dai, S., Jiang, D., 2014. Quantum mechanical basis for kinetic diameters of small gaseous molecules. J. Phys. Chem. A 118, 1150–1154. https://doi.org/10.1021/jp412588f.

Min, M., Seo, S., Yoon, Y., Cho, K., Lee, S.M., Lee, T., Lee, H., 2016. Catalyst-free bottom-up growth of graphene nanofeatures along with molecular templates on dielectric substrates. Nanoscale 8, 17022–17029. https://doi.org/10.1039/C6NR05657A.

Pao, H.-T., Chen, C.-C., 2019. Decoupling strategies: CO2 emissions, energy resources, and economic growth in the group of twenty. J. Clean. Prod. 206, 907–919. https://doi.org/10.1016/J.JCLEPRO.2018.09.190.

Pelletier, C., Rogaume, Y., Dieckhoff, L., Bardeau, G., Pons, M.-N., Dufour, A., 2019. Effect of combustion technology and biogenic CO_2 impact factor on global warming potential of wood-to-heat chains. Appl. Energy 235, 1381–1388. https://doi.org/10.1016/J.APENERGY.2018.11.060.

Peter, S.C., 2018. Reduction of CO_2 to chemicals and fuels: a solution to global warming and energy crisis. ACS Energy Lett 3, 1557–1561. https://doi.org/10.1021/acsenergylett.8b00878.

Pusceddu, E., Montanaro, A., Fioravanti, G., Santilli, S.F., Foscolo, P.U., Criscuoli, I., Raschi, A., Miglietta, F., 2016. Comparison between ancient and fresh biochar samples, a study on the recalcitrance of carbonaceous structures during soil incubation. Int. J. New Technol. Res. 3, 39–46.

Quosai, P., Anstey, A., Mohanty, A.K., Misra, M., 2018. Characterization of biocarbon generated by high- and low-temperature pyrolysis of soy hulls and coffee chaff: for polymer composite applications. R. Soc. Open Sci. 5, 171970. https://doi.org/10.1098/rsos.171970.

Rajapaksha, A.U., Vithanage, M., Ahmad, M., Seo, D.C., Cho, J.S., Lee, S.E., Lee, S.S., Ok, Y.S., 2015. Enhanced sulfamethazine removal by steam-activated invasive plant-derived biochar. J. Hazard. Mater. 290, 43–50. https://doi.org/10.1016/j.jhazmat.2015.02.046.

Rajapaksha, A.U., Chen, S.S., Tsang, D.C.W., Zhang, M., Vithanage, M., Mandal, S., Gao, B., Bolan, N.S., Ok, Y.S., 2016a. Engineered/designer biochar for contaminant removal/immobilization from soil and water: potential and implication of biochar modification. Chemosphere 148, 276–291. https://doi.org/10.1016/j.chemosphere.2016.01.043.

Rajapaksha, A.U., Vithanage, M., Lee, S.S., Seo, D.C., Tsang, D.C.W., Ok, Y.S., 2016b. Steam activation of biochars facilitates kinetics and pH-resilience of sulfamethazine sorption. J. Soils Sediments 16, 889–895. https://doi.org/10.1007/s11368-015-1325-x.

Rathore, P.K.S., Chauhan, D.S., Singh, R.P., 2019. Decentralized solar rooftop photovoltaic in India: on the path of sustainable energy security. Renew. Energy 131, 297–307. https://doi.org/10.1016/J.RENENE.2018.07.049.

Shafeeyan, M.S., Daud, W.M.A.W., Houshmand, A., Shamiri, A., 2010. A review on surface modification of activated carbon for carbon dioxide adsorption. J. Anal. Appl. Pyrolysis 89, 143–151. https://doi.org/10.1016/J.JAAP.2010.07.006.

Shafeeyan, M.S., Daud, W.M.A.W., Houshmand, A., Arami-Niya, A., 2011. Ammonia modification of activated carbon to enhance carbon dioxide adsorption: effect of pre-oxidation. Appl. Surf. Sci. 257, 3936–3942. https://doi.org/10.1016/J.APSUSC.2010.11.127.

Shang, S., Hanif, A., Sun, M., Tian, Y., Ok, Y.S., Yu, I.K.M., Tsang, D.C.W., Gu, Q., Shang, J., 2019. Novel M (Mg/Ni/Cu)-Al-CO3 layered double hydroxides synthesized by aqueous miscible organic solvent treatment (AMOST) method for CO_2 capture. J. Hazard. Mater. 373, 285–293. https://doi.org/10.1016/J.JHAZMAT.2019.03.077.

Shim, T., Yoo, J., Ryu, C., Park, Y.-K., Jung, J., 2015. Effect of steam activation of biochar produced from a giant Miscanthus on copper sorption and toxicity. Bioresour. Technol. 197, 85–90. https://doi.org/10.1016/J.BIORTECH.2015.08.055.

Singh, G., Kim, I.Y., Lakhi, K.S., Srivastava, P., Naidu, R., Vinu, A., 2017. Single step synthesis of activated bio-carbons with a high surface area and their excellent CO_2 adsorption capacity. Carbon N. Y. 116, 448–455. https://doi.org/10.1016/J.CARBON.2017.02.015.

Sizmur, T., Fresno, T., Akgül, G., Frost, H., Moreno-Jiménez, E., 2017. Biochar modification to enhance sorption of inorganics from water. Bioresour. Technol. 246, 34–47. https://doi.org/10.1016/J.BIORTECH.2017.07.082.

Staffell, I., Scamman, D., Velazquez Abad, A., Balcombe, P., Dodds, P.E., Ekins, P., Shah, N., Ward, K.R., 2019. The role of hydrogen and fuel cells in the global energy system. Energy Environ. Sci. https://doi.org/10.1039/C8EE01157E.

Su, F., Lu, C., Kuo, S.-C., Zeng, W., 2010. Adsorption of CO_2 on amine-functionalized Y-type zeolites. Energy Fuel 24, 1441–1448. https://doi.org/10.1021/ef901077k.

Varotsos, C.A., Efstathiou, M.N., 2019. Has global warming already arrived? J. Atmos. Solar-Terrestrial Phys. 182, 31–38. https://doi.org/10.1016/J.JASTP.2018.10.020.

Vilarrasa-García, E., Cecilia, J., Moya, E., Cavalcante, C., Azevedo, D., Rodríguez-Castellón, E., Vilarrasa-García, E., Cecilia, J.A., Moya, E.M.O., Cavalcante, C.L., Azevedo, D.C.S., Rodríguez-Castellón, E., 2015. "Low cost" pore expanded SBA-15 functionalized with amine groups applied to CO_2 adsorption. Materials (Basel) 8, 2495–2513. https://doi.org/10.3390/ma8052495.

Wang, J., Wang, M., Zhao, B., Qiao, W., Long, D., Ling, L., 2013. Mesoporous carbon-supported solid amine sorbents for low-temperature carbon dioxide capture. Ind. Eng. Chem. Res. 52, 5437–5444. https://doi.org/10.1021/ie303388h.

Wei, H., Deng, S., Hu, B., Chen, Z., Wang, B., Huang, J., Yu, G., 2012. Granular bamboo-derived activated carbon for high CO_2 adsorption: the dominant role of narrow micropores. ChemSusChem 5, 2354–2360. https://doi.org/10.1002/cssc.201200570.

Wei, T., Zhang, Q., Wei, X., Gao, Y., Li, H., 2016. A facile and low-cost route to heteroatom doped porous carbon derived from Broussonetia papyrifera bark with excellent supercapacitance and CO_2 capture performance. Sci. Rep. 6, 22646. https://doi.org/10.1038/srep22646.

Woolf, D., Amonette, J.E., Street-Perrott, F.A., Lehmann, J., Joseph, S., 2010. Sustainable biochar to mitigate global climate change. Nat. Commun. 1, 56. https://doi.org/10.1038/ncomms1053.

Xu, X., Kan, Y., Zhao, L., Cao, X., 2016. Chemical transformation of CO_2 during its capture by waste biomass derived biochars. Environ. Pollut. 213, 533–540. https://doi.org/10.1016/J.ENVPOL.2016.03.013.

Yang, J., Zhao, Q., Xu, H., Li, L., Dong, J., Li, J., 2012. Adsorption of CO_2 , CH_4 , and N_2 on gas diameter grade ion-exchange small pore zeolites. J. Chem. Eng. Data 57, 3701–3709. https://doi.org/10.1021/je300940m.

Yang, X., Igalavithana, A.D., Oh, S.-E., Nam, H., Zhang, M., Wang, C.-H., Kwon, E.E., Tsang, D.C.W., Ok, Y.S., 2018. Characterization of bioenergy biochar and its utilization for metal/metalloid immobilization in contaminated soil. Sci. Total Environ., 640–641 https://doi.org/10.1016/j.scitotenv.2018.05.298.

Yu, K.M.K., Curcic, I., Gabriel, J., Tsang, S.C.E., 2008. Recent advances in CO_2 capture and utilization. ChemSusChem 1, 893–899. https://doi.org/10.1002/cssc.200800169.

Zhang, X., Zhang, S., Yang, H., Feng, Y., Chen, Y., Wang, X., Chen, H., 2014. Nitrogen enriched biochar modified by high temperature CO_2–ammonia treatment: characterization and adsorption of CO_2. Chem. Eng. J. 257, 20–27. https://doi.org/10.1016/J.CEJ.2014.07.024.

Zhang, X., Zhang, S., Yang, H., Shao, J., Chen, Y., Feng, Y., Wang, X., Chen, H., 2015. Effects of hydrofluoric acid pre-deashing of rice husk on physicochemical properties and CO2 adsorption performance of nitrogen-enriched biochar. Energy 91, 903–910. https://doi.org/10.1016/J.ENERGY.2015.08.028.